Inorganic Chemistry

Article

Protonated Free-Base Corroles: Acidity, Electrochemistry, and Spectroelectrochemistry of [(Cor)H4]+, [(Cor)H5]2+, and [(Cor)H6]3+

Zhongping Ou,[†,‡] Jing Shen,[‡] Jianguo Shao,[‡,§] Wenbo E,[‡] Michał Gałęzowski,[£]
Daniel T. Gryko,*[£] and Karl M. Kadish*[‡]

Department of Applied Chemistry, Jiangsu University, Zhenjiang 212013 China, Department of Chemistry, University of Houston, Houston, Texas 77204-5003, Department of Chemistry, Midwestern State University, Wichita Falls, Texas 76308, and Institute of Organic Chemistry, Polish Academy of Sciences, Kasprzaka 44/52, 01-224 Warsaw, Poland

Protonated meso-substituted free-base macrocycles of the form [(Cor)H4]+, [(Cor)H5]2+, and [(Cor)H6]3+ where Cor is the trianion of a given corrole, were chemically generated from neutral (Cor)H3 in benzonitrile by addition of trifluoroacetic acid (TFA) and characterized as to their relative acidity, electrochemistry, and spectroelectrochemistry. Three types of protonated free-base corroles with different electron-donating or electron-withdrawing substituents at the meso positions of the macrocycle were investigated. One is protonated exclusively at the central nitrogens of the corrole forming [(Cor)H4]+ from (Cor)H3, while the second and third types of corroles undergo protonation at one or two meso pyridyl substituents prior to protonation of the central nitrogens and give as the final products [(Cor)H5]2+ and [(Cor)H6]3+, respectively. Altogether the relative deprotonation constants (pK_a) for 10 different corroles were determined in benzonitrile and analyzed with respect to the molecular structure and/or type of substituents on the three meso positions of the macrocycle. Mechanisms for oxidation and reduction of the protonated corroles are proposed in light of the electrochemical and spectroelectrochemical data.

Introduction

Numerous spectroscopic and electrochemical characterizations of free-base porphyrins[1] and related macrocycles such as corroles,[2–4] phthalocyanines,[5] chlorins,[6] and porphyrazines[7] have been published in recent years, due in part to the use of these compounds in donor–acceptor systems[8] or a variety of biomedical applications.[9]

Virtually all free-base tetrapyrrolic complexes can be protonated in acidic aqueous or nonaqueous media, leading to formation of partially or fully protonated compounds.[1a,2–5a,6,10–12] Under these conditions, substantial changes will be observed in the electrochemical and spectroscopic properties of the

---

* To whom correspondence should be addressed. E-mail: kkadish@uh.edu (K.M.K.).

† Jiangsu University.

‡ University of Houston.

§ Midwestern State University.

£ Polish Academy of Sciences.

(1) (a) Hambright, P. In *The Porphyrin Handbook*; Kadish, K. M., Smith, K. M., Guilard, R., Eds., Academic Press: Boston, 2000; Vol. 3, Chapter 18, pp 129–210. (b) Inisan, C.; Saillard, J.-Y.; Guilard, R.; Tabard, A.; Mest, Y. L. *New. J. Chem.* **1998**, 823–830. (c) Kadish, K. M.; Caemelbecke, E. V.; Royal, G. In *The Porphyrin Handbook*; Kadish, K. M., Smith, K. M., Guilard, R., Eds., Academic Press: Boston, 2000; Vol. 8, Chapter 8, pp 1–114.

(2) Shen, J.; Shao, J.; Ou, Z.; E, W.; Koszarna, B.; Gryko, D. T.; Kadish, K. M. *Inorg. Chem.* **2006**, *45*, 2251–2265.

(3) Grigg, R.; Hamilton, R. J.; Jozefowicz, M. L.; Rochester, C. H.; Terrell, R. J.; Wickwar, H. *J. Chem. Soc. Perkin Trans. 2* **1973**, 407–416.

(4) Mahammed, A.; Weaver, J. J.; Gray, H. B.; Abdelas, M.; Gross, Z. *Tetrahedron Lett.* **2003**, *44*, 2077–2079.

(5) (a) Liu, J.; Zhao, Y.; Zhao, F.; Zhang, F.; Tang, Y.; Song, X.; Chau, F. T. *Acta. Phys.-Chim.* **1996**, *12*, 202–207. (b) Ishii, K.; Kobayashi, N. In *The Porphyrin Handbook*; Kadish, K. M., Smith, K. M., Guilard, R., Eds.; Academic Press: Boston, 2003; Vol. 16, Chapter 102, pp 1–42. (c) L'Her, M.; Pondaven, A. In *The Porphyrin Handbook*; Kadish, K. M., Smith, K. M., Guilard, R., Eds., Academic Press: Boston, 2003; Vol. 16, Chapter 104, pp 117–169.

(6) Kruk, M. M.; Braslavsky, S. E. *J. Phys. Chem.* **2006**, *110*, 3414–3425.

(7) Donzello, M. P.; Ou, Z.; Monacelli, F.; Ricciardi, G.; Rizzoli, C.; Ercolani, C.; Kadish, K. M. *Inorg. Chem.* **2004**, *43*, 8626–8636.

(8) (a) Fukuzumi, S.; Ohdubo, K.; Imahori, H.; Shao, J.; Ou, Z.; Zheng, G.; Chen, Y.; Randey, R. K.; Fujitsuka, M.; Ito, O.; Kadish, K. M. *J. Am. Chem. Soc.* **2001**, *123*, 10676–10683. (b) Flamigni, L.; Talarico, A. M.; Barigelletti, F.; Johnston, M. R. *Photochem. Phtotbiol. Sci.* **2002**, *1*, 190–197. (c) Pettersson, K.; Kyrychenko, A.; Rönnow. E.; Ljungdahl, T.; Mårtensson, J.; Albinsson, B. *J. Phys. Chem. A* **2006**, *110*, 310–318. (d) D'Souza, F.; Chitta, R.; Gadde, S.; Zandler, M. E.; McCarty, A. L.; Sandanayaka, A. S. D.; Araki, Y.; Ito, O. *J. Phys. Chem. A* **2006**, *110*, 4338–4347. (e) Eng, M. P.; Ljungdahl, T.; Mårtensson, J.; Albinsson, B. *J. Phys. Chem. A* **2006**, *110*, 6483–6491. (f) Takagi, S.; Eguchi, M.; Tryk, D. A.; Inoue, H. *Langmuir* **2006**, *22*, 1406–1408.

compounds, thus potentially making them either more or less effective in a variety of applications.
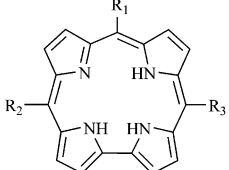
Our own interest in free-base tetrapyrroles has recently focused in part on the electrochemistry and UV–visible spectra of protonated free-base corroles in nonaqueous media.[2] The current work examines the acid–base properties and UV–visible spectra of protonated free-base corroles and provides the first comprehensive study of deprotonation constants for these compounds in a nonaqueous solvent.

To our knowledge deprotonation constants for only three [(Cor)H$_4$]$^+$ derivatives have been reported in the literature. One compound was examined in aqueous media[4] and two in toluene.[3] There have been no systematic measurements of pK_a values for protonated free-base corroles with different structures or different basicities of the macrocycles. There have also been no measurements of pK_a values for free-base corroles where protonation can occur at multiple sites of the macrocycle. This is addressed in the current paper where 10 protonated free-base corroles with different electron-donating or electron-withdrawing groups at the three meso positions of the macrocycle were characterized as to their pK_a values in the nonaqueous solvent, benzonitrile. The investigated compounds are listed in Chart 1 and are divided into three groups based on the number of pyridyl substituents at the meso position of the corrole macrocycle. The first group of compounds (**1**–**7**) undergoes protonation exclusively at the central nitrogens leading to formation of [(Cor)H$_4$]$^+$ while the second (compounds **8** and **9**) and third (compound **10**) show protonation at one or two pyridyl substituents of the macrocycle prior to protonation of the central nitrogens.

The examined corroles from the first group of compounds can be further subdivided into compounds with nonhindered or hindered meso substituents, and this is done in Chart 1 where the compounds in group A are listed under the subcategory A-1 or A-2 and arranged according to the electron-donating or electron-withdrawing effect of the meso substituents, as described by the $\Sigma\sigma$ values.[13] As will be demonstrated, the pyridyl substituents on compounds **8**, **9**, and **10** are protonated prior to protonation of the central nitrogens, thus leading to the stepwise formation of [(Cor)H$_4$]$^+$ and [(Cor)H$_5$]$^{2+}$ in the case of **8** and **9** and [(Cor)H$_4$]$^+$, [(Cor)H$_5$]$^{2+}$, and [(Cor)H$_6$]$^{3+}$ in the case of **10**.

Each protonated corrole was chemically generated by addition of trifluoroacetic acid (TFA) to the corresponding neutral free-base compound, (Cor)H$_3$, and the progress of the reaction followed by UV–visible spectroscopy and electrochemistry. The spectroscopic data were then analyzed as a function of TFA concentration, and the relative

Chart 1

group type[a]	compound	R$_1$	R$_2$	R$_3$
A-1	1	Me—⟨C$_6$H$_4$⟩—	Me—⟨C$_6$H$_4$⟩—	Me—⟨C$_6$H$_4$⟩—
	2	F$_3$C—⟨C$_6$H$_4$⟩—	F$_3$C—⟨C$_6$H$_4$⟩—	F$_3$C—⟨C$_6$H$_4$⟩—
	3	NC—⟨C$_6$H$_4$⟩—	NC—⟨C$_6$H$_4$⟩—	NC—⟨C$_6$H$_4$⟩—
	4	(F$_3$C)$_2$C$_6$H$_3$—	(F$_3$C)$_2$C$_6$H$_3$—	(F$_3$C)$_2$C$_6$H$_3$—
A-2	5	NC—⟨C$_6$H$_4$⟩—	Me$_3$C$_6$H$_2$—	Me$_3$C$_6$H$_2$—
	6	NC—⟨C$_6$H$_4$⟩—	Cl$_2$C$_6$H$_3$—	Cl$_2$C$_6$H$_3$—
	7	C$_6$F$_5$—	C$_6$F$_5$—	C$_6$F$_5$—
B	8	⟨pyridyl⟩—	Me$_3$C$_6$H$_2$—	Me$_3$C$_6$H$_2$—
	9	⟨pyridyl⟩—	Cl$_2$C$_6$H$_3$—	Cl$_2$C$_6$H$_3$—
C	10	F$_2$C$_6$H$_3$—	⟨pyridyl⟩—	⟨pyridyl⟩—

[a] Group type: A-1 represents corroles with nonhindered meso substituents, group A-2 represents corroles with sterically hindered meso substituents, and groups B and C represent corroles with one and two pyridyl meso substituents, respectively.

deprotonation constants (pK_a) calculated using equations described in the text.

The doubly and triply protonated compounds **8**, **9**, and **10** have not previously been studied in detail and each was characterized in the present paper as to their redox properties and UV–visible spectra before and after the addition or abstraction of electrons.

Experimental Section

Chemicals. The investigated free-base corroles were synthesized as described in the literature.[14–16] TFA (99+%) was purchased from Aldrich Chemical Co. and used as received. Benzonitrile (PhCN) was obtained from Aldrich Co. and was distilled over P$_2$O$_5$ under vacuum prior to use. Tetra-n-butylammonium perchlorate (TBAP) was purchased from Fluka Chemika Co.,

(9) (a) Wei, C.; Jia, G.; Yuan, J.; Feng, Z.; Li, C. *Biochem.* **2006**, *45*, 6681–6691. (b) Ben-hur, E.; Chan, W.-S. In *The Porphyrin Handbook*; Kadish, K. M., Smith, K. M., Guilard, R., Eds.; Academic Press: Boston, 2003; Vol. 19, Chapter 117, pp 1–35. (c) Pandy, R.; Zhang, G. In *The Porphyrin Handbook*; Kadish, K. M., Smith, K. M., Guilard, R., Eds.; Academic Press: Boston, 2000; Vol. 6, Chapter 43, pp 157–230.
(10) Karaman, R.; Bruice, T. C. *Inorg. Chem.* **1992**, *31*, 2455–2459.
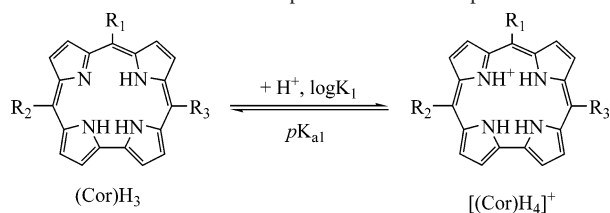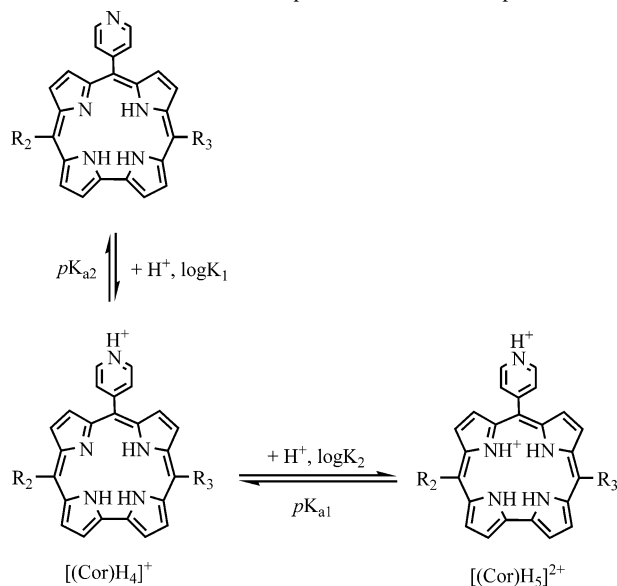(11) Aronoff, S. *J. Phys. Chem.* **1958**, *62*, 428–431.
(12) Sutter, T. P. G.; Hambright, P. *Inorg. Chem.* **1992**, *31*, 5089–5093.
(13) Hansch, C.; Leo, A.; Taft, R. W. *Chem. Rev.* **1991**, *91*, 165–195.

(14) Gryko, D. T.; Piechota, K. E. *J. Porphyrins Phthalocyanines* **2002**, *6*, 81–97.
(15) Gryko, D. T.; Koszarna, B. *Org. Biomol. Chem.* **2003**, *1*, 350–357.
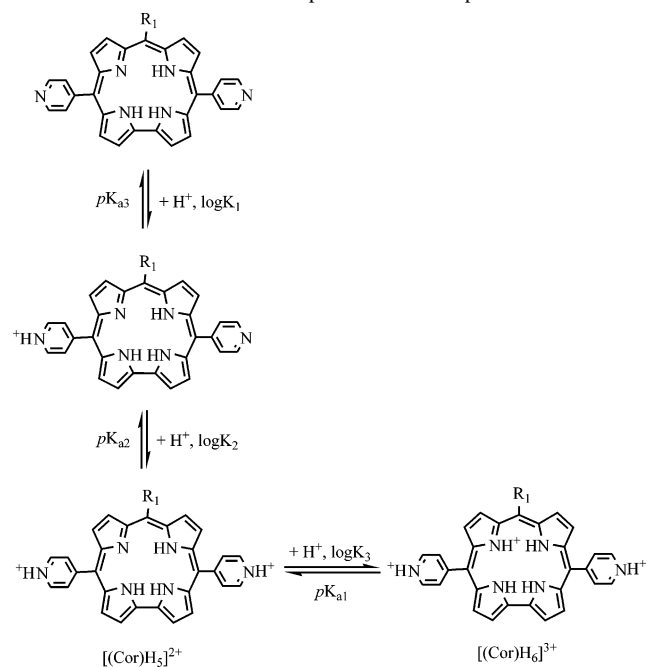(16) Gryko, D. T.; Jadach, K. *J. Org. Chem.* **2001**, *66*, 4267–4275.

Scheme 1. Protonation of Compounds **1**−**7** in Group A

Scheme 2. Protonation of Compounds **8** and **9** in Group B

Scheme 3. Protonation of Compound **10** in Group C

investigated compounds is schematically illustrated in Schemes 1−3 and the individual protonation steps in the three schemes are given by eqs 1−3.

$$(Cor)H_3 + CF_3COOH \overset{K_1}{\rightleftharpoons} [(Cor)H_4]^+ + CF_3COO^- \quad (1)$$

$$[(Cor)H_4]^+ + CF_3COOH \overset{K_2}{\rightleftharpoons} [(Cor)H_5]^{2+} + CF_3COO^- \quad (2)$$

$$[(Cor)H_5]^{2+} + CF_3COOH \overset{K_3}{\rightleftharpoons} [(Cor)H_6]^{3+} + CF_3COO^- \quad (3)$$

Each of the above reactions involves a combination of deprotonation reactions for CF_3COOH in benzonitrile (eq 4) and the specific corrole, $[(Cor)H_4]^+$, $[(Cor)H_5]^{2+}$, or $[(Cor)H_6]^{3+}$ under the same solution conditions, the latter of which is given by eq 5 for the individual compounds **1**−**7**

$$CF_3COOH \overset{K_a'}{\rightleftharpoons} CF_3COO^- + H^+ \quad (4)$$

$$[(Cor)H_4]^+ \overset{K_{a1}}{\rightleftharpoons} (Cor)H_3 + H^+ \quad (5)$$

where

$$K_1 = K_a'/K_{a1} \quad (6)$$

and

$$pK_{a1} = pK_a' + \log K_1 \quad (7)$$

A similar mathematical relationship exists between the experimentally measured K_2 (eq 2) and K_3 (eq 3) values for compounds **8**, **9**, and **10** and the calculated nonaqueous pK_{a2} and pK_{a3} values for the second and third protonation steps of these compounds. In this regard, it should be pointed out that a pK_a' for CF_3COOH is not available in benzonitrile and the literature value of 0.23

recrystallized from ethyl alcohol, and dried under vacuum at 40 °C for at least one week prior to use.

Instrumentation. Cyclic voltammetry was carried out with an EG&G Princeton Applied Research (PAR) 173/273 potentiostat/ galvanostat. A homemade three-electrode cell was used for cyclic voltammetric measurements and consisted of a glassy carbon working electrode, a platinum counter electrode, and a homemade saturated calomel reference electrode (SCE). The SCE was separated from the bulk of the solution by a fritted glass bridge of low porosity which contained the solvent/supporting electrolyte mixture. Thin-layer UV−visible spectroelectrochemical experiments were performed with a home-built thin-layer cell which had a light transparent platinum net working electrode.[17] Potentials were applied and monitored with an EG&G PAR Model 173 potentiostat. Time-resolved UV−visible spectra were recorded with a Hewlett-Packard Model 8453 diode array spectrophotometer.

Determination of Nonaqueous pK_a Values. Equilibrium constants ($\log K$) of the protonation reactions were measured at room temperature. The Hill equation, which analyzes changes in UV−visible spectra during the titration as a function of the concentration of added reactant,[18] was used to calculate the equilibrium constant ($\log K$)[19] which enabled calculation of relative pK_a values for all 10 corroles in the nonaqueous solvent, PhCN.
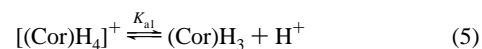
For compounds **1**−**7**, only the central nitrogens of the corroles can be protonated, while in the case of compounds **8**, **9**, and **10**, protonation first occurs at the meso pyridyl substituents, followed at higher concentrations of added CF_3COOH by protonation of the central nitrogens. The overall sequence of reactions for the

(17) Lin, X. Q.; Kadish, K. M. *Anal. Chem.* **1985**, *57*, 1498−1501.
(18) Brault, D.; Rougee, M. *Biochem.* **1974**, *13*, 4591−4597.
(19) Ellis, P. E.; Linard, J. E.; Szymanski, T.; Jones, R. D.; Budge, J. R.; Basolo, F. *J. Am. Chem. Soc.* **1980**, *102,* 1889−1896.
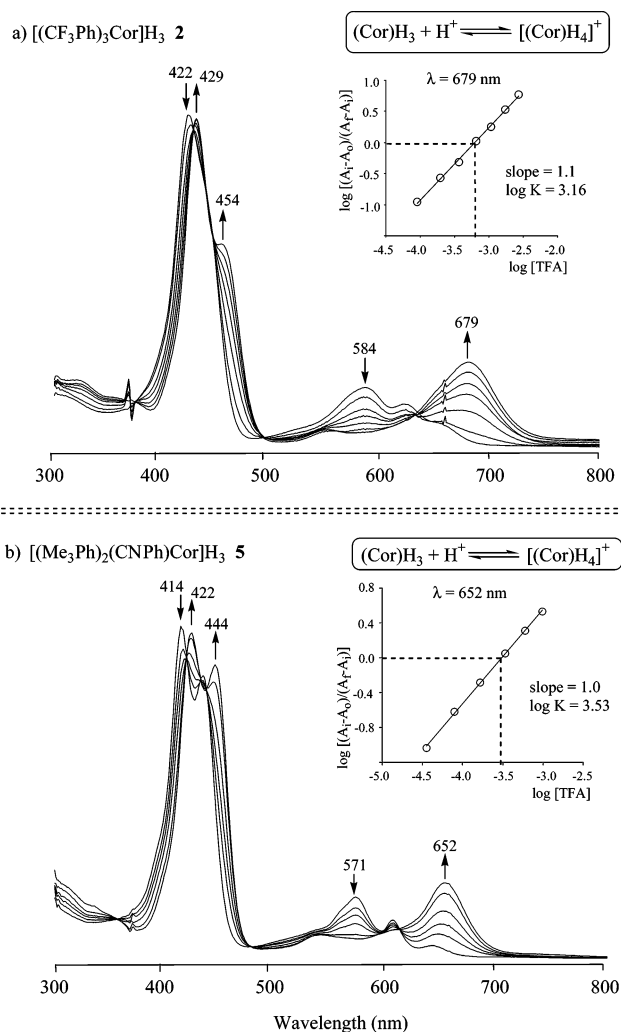
measured in aqueous solution[20] was therefore utilized in the calculation. This replacement is not of major importance, however, since the "true" aqueous pK_a cannot be obtained and the magnitude of the relative pK_a values for the 10 corroles are all shifted by a similar amount in the nonaqueous solvent, PhCN.

Results and Discussion

Spectroscopic Monitoring of $(Cor)H_3$ Protonation for Compounds 1−7. The presence or absence of sterically hindered meso substituents on the corroles in group A is reflected in slightly different UV−visible spectra, as previously discussed in the literature.[2] The group A-1 $(Cor)H_3$ derivatives in Chart 1 with nonhindered substituents (1−4) have a Soret band at 421−424 nm and two major visible bands located at ∼584 and 620 nm in PhCN (Figure S1), while the group A-2 corroles with sterically hindered substituents (5−7, Figure S2) have a split Soret band with maxima at 413−416 nm, a shoulder at ∼432 nm, and two major visible bands located between 566 and 571 and 605 and 609 nm under the same solution conditions. A comparison of the two types of UV−vis spectra is given for $[(CF_3Ph)_3Cor]H_3$ (2) and $[(Me_3Ph)_2(CNPh)Cor]H_3$ (5) in Figure 1, and this figure also shows the spectral changes obtained during protonation of the two corroles as TFA is added to the PhCN solution.

Compound 2 in group A-1 has three nonsterically hindered $C_6H_4(CF_3)$ meso substituents, while compound 5 in group A-2 has two sterically hindered meso mesityl $(C_6H_2(CH_3)_3)$ substituents. Both corroles undergo only a slight (7−8 nm) red-shift in λ_{max} of the Soret band as TFA is added to the PhCN solution forming $[(Cor)H_4]^+$, and there is no significant change in the molar absorptivity of this band upon protonation (see Figure 1). In addition, the two visible bands in the spectrum of the neutral corrole disappear upon conversion of $(Cor)H_3$ to $[(Cor)H_4]^+$ and these are replaced by a more intense visible band located at 679 and 652 nm for 2 and 5, respectively. The exact position of this latter band for all of the group A corroles is summarized in Table 1 and seems to correlate with the steric hinderence of the meso substituents, i.e., λ_{max} ranges from 671 to 694 nm for the group A-1 compounds and from 632 to 652 nm for the group A-2 compounds.

The spectral data during titration of each corrole with TFA were analyzed by the Hill equation,[19] and examples of the relevant plots are shown in the insets of Figure 1a and b for 2 and 5. A linear relationship between $\log[(A_i - A_o)/(A_f - A_i)]$ and $\log[TFA]$ is obtained for both compounds, with a slope of ∼1.0, thus indicating that only one proton is added to $(Cor)H_3$, giving $[(Cor)H_4]^+$ as shown in eq 1 and Scheme 1. The calculated equilibrium constant is 3.16 for compound 2 and 3.53 for compound 5. These values are labeled as log K_{CN} (CN = central nitrogen) in Table 1 along with the measured equilibrium constants and $pK_{a(CN)}$ values for the other five corroles in groups A-1 and A-2. The largest H$^+$ binding constant in the group A compounds is for compound

(20) Weast, R. C.; Astle, M. J.; Beyer, W. H. *Handbook of Chemistry and Physics*, 66th ed.; CRC Press, Inc.: Boca Raton, FL, 1985−1986.

Figure 1. UV−visible spectral changes during protonation of (a) compound 2 (7.71×10^{-6} M) and (b) compound 5 (6.26×10^{-6} M) by addition of TFA in PhCN.

1 (log K_{CN} = 4.33, $pK_{a(CN)}$ = 4.56) and the smallest for compound 7 (log K_{CN} = 1.54, $pK_{a(CN)}$ = 1.77).

Stepwise Protonation of $(Cor)H_3$ to Give $[(Cor)H_4]^+$, $[(Cor)H_5]^{2+}$, and $[(Cor)H_6]^{3+}$. Compounds 8 and 9. These two corroles differ from compounds 1−7 in that they contain an easily protonated pyridyl group at the R_1 position of the macrocycle (see Chart 1). The protonation reactions for 8 and 9 each involves a well-defined two-step process, as shown in Scheme 2, and the spectral changes obtained as a function of increasing [TFA] are shown in Figure 2 for the case of compound 8. Similar spectral changes are seen during the two-step protonation of compound 9.

The UV−visible spectrum of singly protonated 8 and 9 differs from that of the singly protonated corroles 1−7 in that the Soret band of the monopyridyl corroles is significantly decreased in intensity and has also undergone a significant red-shift, as compared to only modest changes in the Soret band position and molar absorptivity after protonation of the other corroles lacking a meso-substituted pyridyl group.

The difference in UV−visible spectra between the mono-protonated 8 or 9 and the monoprotonated 1−7 derivatives

Table 1. Equilibrium Constants for Protonation of Central Nitrogens (log $K_{(CN)}$) and Spectroscopic/Electrochemical Data of Fully Protonated Corroles in PhCN

group type	compd	formula	inner core nitrogens (CN)		$\lambda_{max}{}^a$	$E_{1/2}$ (ox)^b	$\sum \sigma$
			log $K_{(CN)}$	p$K_{a(CN)}$			
A-1	1	[((MePh)₃Cor)H₄]⁺	4.33	4.56	694	0.60	−0.51
	2	[((CF₃Ph)₃Cor)H₄]⁺	3.16	3.39	679	0.77	1.62
	3	[((CNPh)₃Cor)H₄]⁺	3.05	3.28	677	0.79	1.68
	4	[(((CF₃)₂Ph)₃Cor)H₄]⁺	2.41	2.64	671	0.88	2.58
A-2	5	[((CNPh)(Me₃Ph)₂Cor)H₄]⁺	3.53	3.76	652	0.75	−0.36
	6	[((CNPh)(Cl₂Ph)₂Cor)H₄]⁺	2.48	2.71	647	0.84	1.46
	7	[((F₅Ph)₃Cor)H₄]⁺	1.54	1.77	632	1.04	3.66
B	8	[((pyH⁺)(Me₃Ph)₂Cor)H₄]²⁺	2.38	2.61	651	0.86	c
	9	[((pyH⁺)(Cl₂Ph)₂Cor)H₄]²⁺	1.71	1.94	646	0.98	c
C	10	[((pyH⁺)₂(F₂Ph)Cor)H₄]³⁺	0.80	1.03	681	1.10	c

^{a} Full spectrum given in Figures S1−S2. ^{b} $E_{1/2}$ for **1**−**7** taken from ref 2. ^{c} $\sum \sigma$ values are not available for compounds with pyridyl groups at the meso position of the corrole.
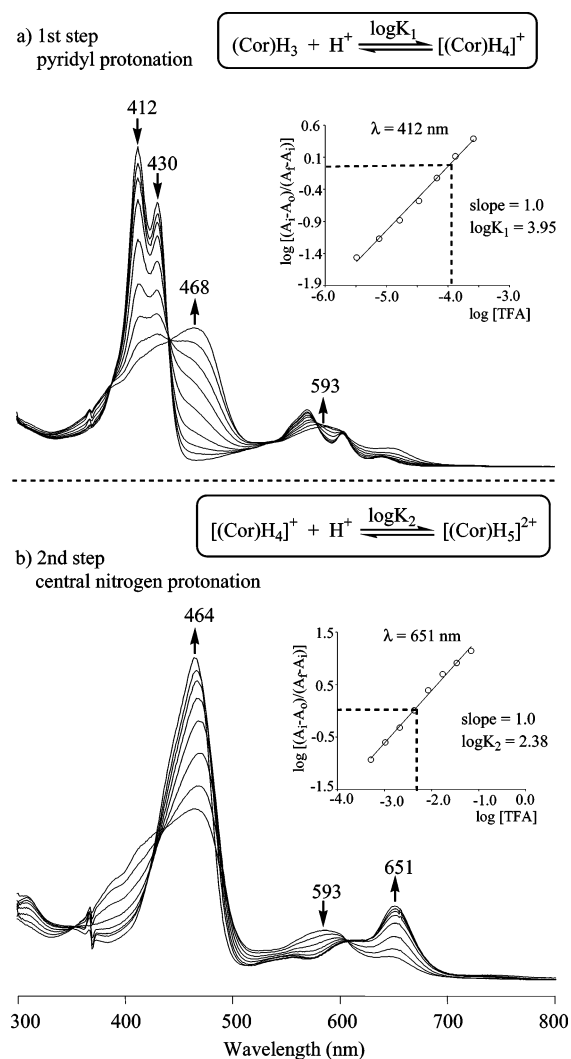
Figure 2. UV−visible spectral changes during the stepwise protonation of 1.84×10^{-5} M ((Me₃Ph)₂(py)Cor)H₃ (**8**) by addition of TFA in PhCN. (a) The first step involves protonation of the pyridyl group ([TFA] from 0 to 2.60×10^{-4} M), and (b) the second protonation of the inner nitrogens ([TFA] from 2.60×10^{-4} to 6.92×10^{-2} M).

is consistent with the first proton addition to **8** and **9** occurring at the nitrogen of the meso pyridyl substituent, and this protonation step is then followed at higher TFA concentrations by formation of [(Cor)H₅]²⁺ where the second proton has been added to the central nitrogens of the

macrocycle as shown in Scheme 2. This second protonation step, like the first, has well-defined isosbestic points as illustrated in Figure 2b for compound **8** where the final spectrum has two major absorption bands at 464 and 651 nm. The wavelength of the latter band is almost identical to a band at 652 nm for [(Cor)H₄]⁺ (**5**) (Figure 1b), and this similarity in λ_{max} can be accounted for by the similar structures of the two corroles, i.e., both **5** and **8** have mesityl groups at the R_2 and R_3 meso positions of the macrocycle (see Chart 1).

The stepwise protonation constants of **8** as shown in Scheme 2 were calculated as log K_1 = 3.95 and log K_2 = 2.38 from the Hill plots shown in the insets of Figure 2. A similar calculation for compound **9** gave log K_1 = 4.53 and log K_2 = 1.71. The second proton addition to **8** and **9** (log K_2) occurs at the central nitrogens of the macrocycle in each case, and the measured equilibrium constants are labeled as log $K_{(CN)}$ in Table 1 for comparison with the other compounds.

Compound 10. This corrole has meso-substituted pyridyl groups at the R_2 and R_3 positions of the macrocycle and can accept three protons in total, one at the each nitrogen of the two pyridyl groups and one at the central nitrogens of the macrocycle. The three protonation steps are schematically shown in Scheme 3, and each was spectrally monitored during a titration with TFA, giving the spectral changes illustrated in Figure 3. Each of the three proton additions is accompanied by well-defined isosbestic points and analysis of the data gives log K_1 = 4.34, log K_2 = 3.25, and log K_3 = 0.80 (Table 2). The third protonation of **10**, which occurs at the central nitrogens (log K_3) is also included in Table 1 and labeled as log $K_{(CN)}$.

UV−Visible Spectra Features of [(Cor)H₄]⁺, [(Cor)H₅]²⁺, and [(Cor)H₆]³⁺. Figure 4 compares the UV−visible spectra of fully protonated [(Cor)H₄]⁺ (**2** and **6**), [(Cor)H₅]²⁺ (**9**), and [(Cor)H₆]³⁺ (**10**) in PhCN. Compounds **2** and **6** are protonated at the central nitrogen atoms, while compounds **9** and **10** have one and two additional protons at the meso pyridyl substituents of the corrole, respectively, in addition to a protonation of the central nitrogens. The sterically hindered corroles **6** and **9** in Figure 4b have similar C₆H₃Cl₂ substituents at the R_2 and R_3 positions of the
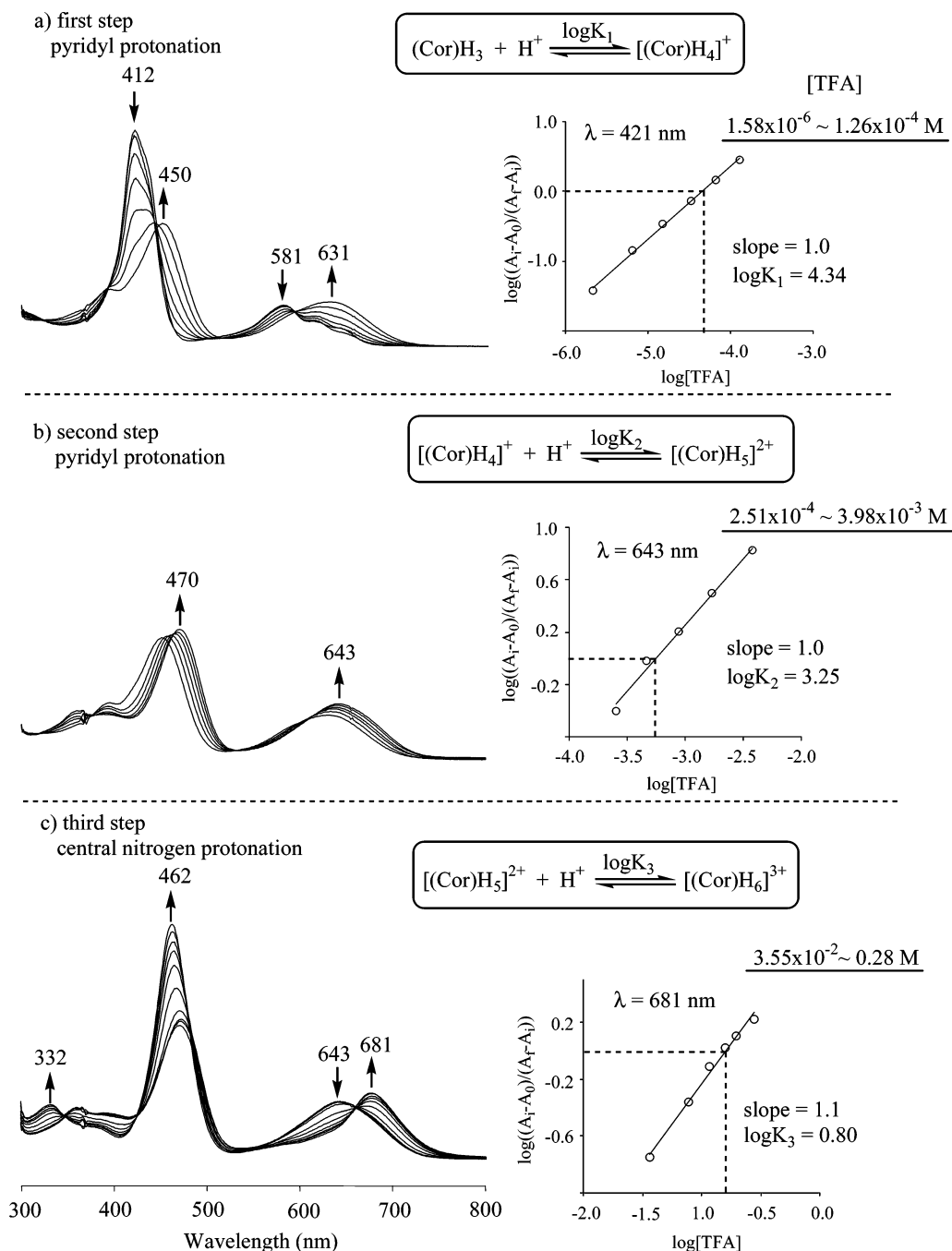
Figure 3. UV−visible spectral changes of 1.14×10^{-5} M $[(F_2Ph)(py)_2Cor]H_3$ (**10**) in PhCN upon the first, second, and third protonation during addition of TFA.

**Table 2.** Stepwise Equilibrium Constants (log K) for Protonation of Groups B and C Corroles in PhCN[a]

group type	compd	first step		second step		third step	
		log K_1	pK_a	log K_2	pK_a	log K_3	pK_a
B	**8**	3.95	4.18	2.38	2.61		
	9	4.53	4.76	1.71	1.94		
C	**10**	4.34	4.57	3.25	3.48	0.80	1.03

[a] The last protonation step in each case occurs at the central nitrogens of the macrocycle, as shown in Schemes 2 and 3.

macrocycle, and they also have virtually the same visible band at $\lambda_{max} = 646-647$ nm for the mono- and diprotonated corroles, respectively. In a like manner, the wavelength maximum for the visible bands of the nonsterically hindered

monoprotonated corrole **2** and triprotonated corrole **10** in Figure 4a are also virtually superimposable, namely $\lambda_{max} = 679$ nm for **2** and 681 nm for **10**.

The intense visible bands between 646 and 681 nm for the compounds in Figure 4 are diagnostic for central nitrogen protonation of the investigated corroles, and the position of the Soret band is also characteristic for protonation of the pyridyl groups. This is seen by comparison of the spectral data for the protonated forms of **8**, **9**, and **10** which is given in Table 3. The group C corrole $[(Cor)H_6]^{3+}$ (**10**) has a Soret band maximum at 462 nm, while the group B corroles $[(Cor)H_5]^{2+}$ (**9**) and $[(Cor)H_5]^{2+}$ (**8**) have a Soret band at 459 and 464 nm, respectively. In all three cases, the Soret
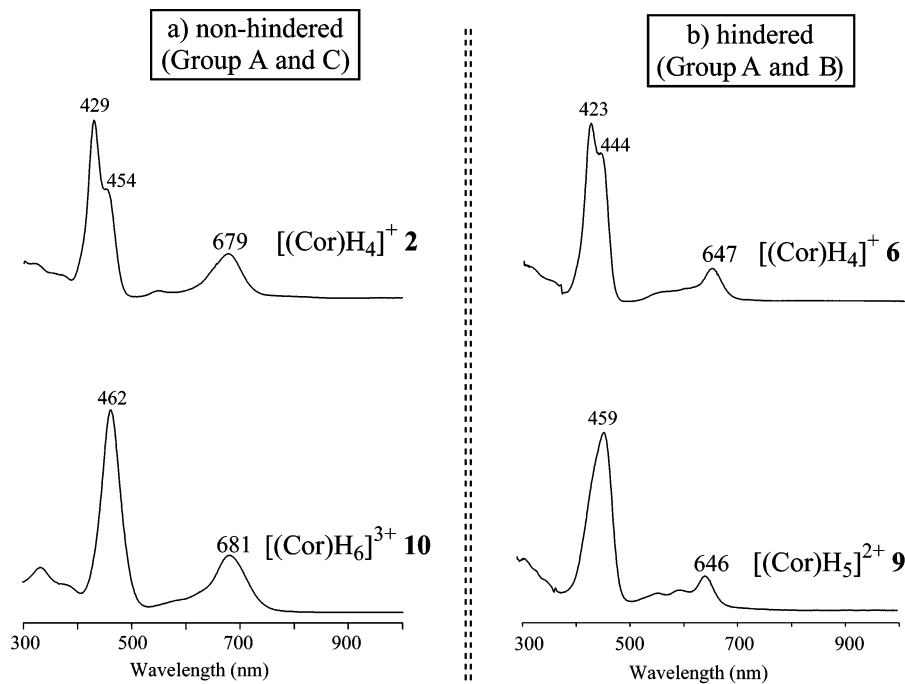
Figure 4. UV−visible spectra of $[(Cor)H_4]^+$, $[(Cor)H_5]^{2+}$, and $[(Cor)H_6]^{3+}$ in PhCN for selected compounds with (a) nonsterically and (b) sterically hindered substituents.

Table 3. UV−Visible Spectral Data (λ_{max}, nm, $\epsilon \times 10^{-4}$ M^{-1} cm^{-1}) of Neutral and Protonated Group B and C Corroles in PhCN

group type	compd	form	Soret band[a]		visible bands	
B	8	$(Cor)H_3$	412 (7.5)	430 (6.3)	570 (1.3)	604 (0.9)
		$[(Cor)H_4]^+$	468 (3.7)		593 (0.9)	
		$[(Cor)H_5]^{2+}$	464 (6.1)		651 (1.2)	
	9	$(Cor)H_3$	414 (10.0)	430 (8.5)	571 (1.8)	609 (1.1)
		$[(Cor)H_4]^+$	463 (4.8)		577 (1.6)	
		$[(Cor)H_5]^{2+}$	459 (9.3)		646 (1.8)	
C	10	$(Cor)H_3$	421 (8.3)	437 (6.1)s	581 (1.6)	612 (1.0)
		$[(Cor)H_4]^+$	450 (4.7)		631 (1.7)	
		$[(Cor)H_5]^{2+}$	470 (5.0)		643 (2.2)	
		$[(Cor)H_6]^{3+}$	462 (8.9)		681 (2.5)	

[a] s = shoulder peak.

band maximum in PhCN containing TFA is shifted by 41−45 nm as compared to the same compounds in neat PhCN where no protonation of the pyridyl groups has occurred, i.e., λ_{max} = 412, 414, and 421 nm for **8**, **9**, and **10**, respectively as seen in Figure S3 and Table 3.

The Soret band maximum of the seven group A non-pyridyl-containing corroles in acidic media varies from 420 to 429 nm (see Figures S1 and S2) and is dependent only on the steric hindrance of the meso substituents at the R_1, R_2, and R_3 positions of the macrocycle. In summary, the shift of λ_{max} of the Soret band from 413 to 429 nm in neat PhCN to 459−464 nm is clearly diagnostic for protonation of the pyridyl groups while the appearance of a visible band at 632−681 nm, which is not seen for the same compounds in neat PhCN, is diagnostic for protonation of the central nitrogens. Both features are present in compounds **8**, **9**, and **10** where multiple protonation occurs.

Electrochemistry of Fully Protonated Corroles. Cyclic voltammograms illustrating the first oxidation and first or second reduction of the fully protonated corroles are shown
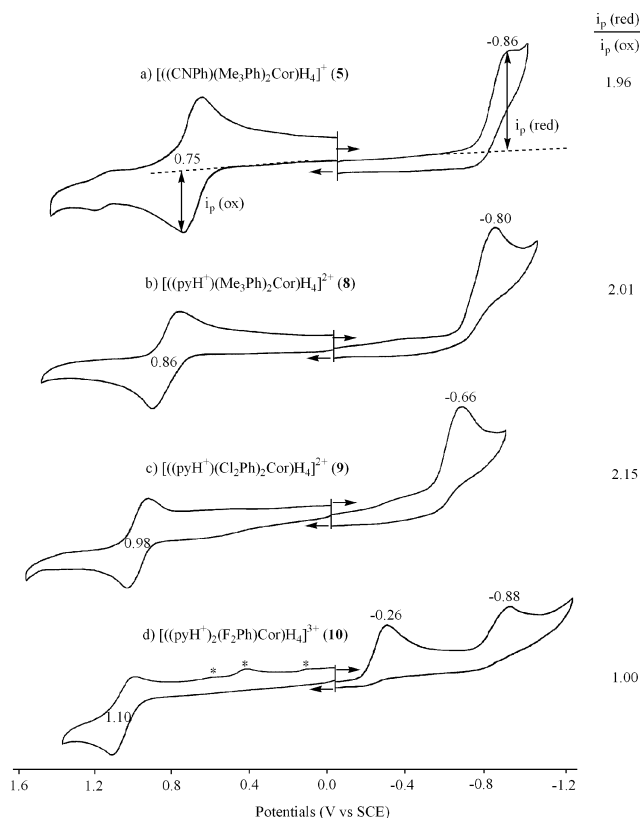

Figure 5. Cyclic voltammograms of fully protonated corroles in PhCN with added TFA at a scan rate of 0.1V/s. Peaks indicated by an asterisk are "decomposition products" of the first oxidation.

in Figure 5 for **5** (group A), **8** and **9** (group B), and **10** (group C). A reversible one-electron oxidation is observed for all four corroles in the three groups, but a slow chemical reaction follows the abstraction of one electron from the group C corrole **10**. This EC-type mechanism (electron transfer

followed by chemical reaction) is characterized by a decreased cathodic peak current for re-reduction of the singly oxidized species at $E_{1/2} = 1.10$ V and the presence of small re-reduction peaks labeled by an asterisk in Figure 5d and located at $E_p = 0.64$, 0.46, and 0.15 V for a scan rate of 0.1 V/s. The nature of the chemical reaction is discussed in a following section of the manuscript which presents UV–visible spectra obtained after controlled potential oxidation of **8**, **9**, and **10** in PhCN containing added TFA.

Compound **10** differs from compounds **5**, **8**, and **9** not only in its oxidation properties but also in its reduction. As seen in Figure 5, the triply protonated corrole undergoes two irreversible one-electron reductions at $E_p = -0.26$ and -0.88 V for a scan rate of 0.1 V/s while **5**, **8**, and **9** show only a single irreversible reduction at the same scan rate. The single reduction of **5**, **8**, and **9** seems to involve two or more electrons on the basis of the peak currents which are approximately double those of the oxidations. The higher reduction peak currents for these compounds contrasts with the case of **10** where each of the two irreversible reductions has almost an identical peak current as the single irreversible oxidation at a scan rate of 0.1 V/s. This is true for both the first reduction at $E_{pc} = -0.26$ and the second reduction at $E_{pc} = -0.88$ V where, in each case, $i_{p(red)}/i_{p(ox)} \approx 1.0$.

In our initial study of $[(Me_3Ph)_2(CNPh)Cor]H_3$ (**5**), it was reported that $i_{p(red)}/i_{p(ox)} = 1.0$ in solutions containing 8.0 equiv of TFA.[2] However, further studies of the same corrole in PhCN solutions show that the ratio of reduction to oxidation peak currents actually depends upon the concentration of TFA added to solution, with the $i_{p(red)}/i_{p(ox)}$ ratio varying from 1.0 at less than 10 equiv of TFA to >2.0 at higher TFA concentration. Similar, but not identical, behavior is also seen for **8** and **9** where the $i_{p(red)}/i_{p(ox)}$ ratio is always ≥ 2.0 under conditions where the fully protonated $[(Cor)H_5]^{2+}$ derivatives are formed. Thus, on one hand, there appears to be three distinct types of redox behavior for the fully protonated corroles **5**, **8**, **9**, and **10**: compound **5**, where the $i_{p(red)}/i_{p(ox)}$ ratio varies from 1.0 to 2.2, compounds **8** and **9**, where $i_{p(red)}/i_{p(ox)} \geq 2$, and compound **10**, where $i_{p(red)}/i_{p(ox)} = 1.0$. However, less distinction between the reductive behavior of the compounds is seen if one compares the total current for the two reductions of **10** to that for the single reduction of **5**, **8**, and **9**. Using this analysis, the main differences between the compounds can be described in terms of the peak potentials for reduction, and these are largely dependent on the nature of the substituents and overall charge of the compound being reduced. This is shown graphically in Figure 6 where peak potentials for the reduction of $[(Cor)H_2]^-$, $(Cor)H_3$, and the three protonated forms of the corrole are plotted as a function of charge on the overall complex which varies from -1 in the case of $[(Cor)H_2]^-$ to $+3$ in the case of $[(Cor)H_6]^{3+}$. The nature of the meso substituents influence in each case the exact potential value for a given corrole, but when considering all of the data, one can conclude that each unit increase in positive charge on the corrole results in an approximate 350 mV shift toward easier reduction. There is also an overall difference of almost 1.5 V in E_p for
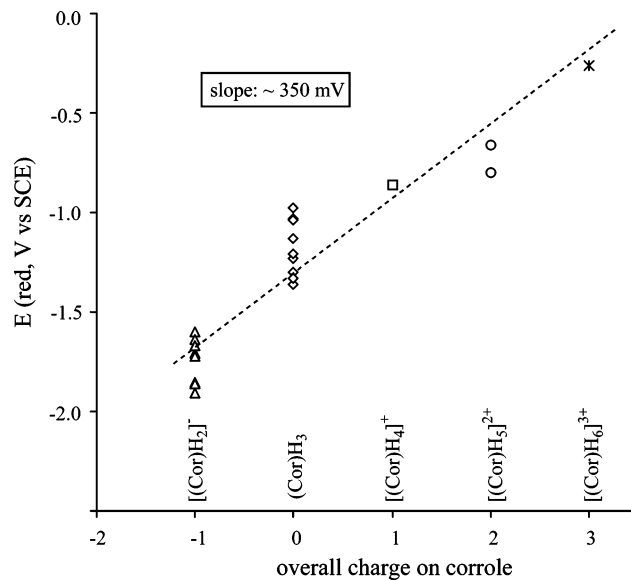
Figure 6. Relationship between reduction peak potentials and overall charge on the corrole. The reduction potentials of $[(Cor)H_2]^-$ and $(Cor)H_3$ in PhCN are taken from ref 2.

Scheme 4. Overall Reduction Mechanism for Fully Protonated Corroles in PhCN
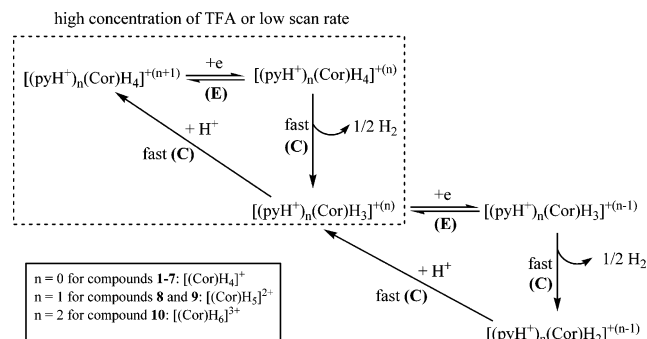
the ring reduction of $[(Cor)H_2]^-$ and the ring reduction of $[(Cor)H_6]^{3+}$, with the latter compound being the easiest to reduce.

As shown in the present study, the reductions of $[(Cor)H_4]^+$ (**1–7**), $[(Cor)H_5]^{2+}$, (**8** and **9**) and $[(Cor)H_6]^{3+}$ (**10**) in PhCN remain irreversible, independent of the potential sweep rate or acid concentration in solution. An irreversible reduction of $(Cor)H_3$ to generate $[(Cor)H_2]^-$ was also observed in neat PhCN without added acid as described in an earlier publication.[2] This initial electron addition occurs at the conjugated macrocycle and is followed by a catalytic reduction of one proton of the $(Cor)H_3$ macrocycles. We propose that a similar catalytic reduction of H^+ also occurs after the one-electron reduction of $[(Cor)H_4]^+$ (**1–7**), $[(Cor)H_5]^{2+}$ (**8** and **9**), and $[(Cor)H_6]^{3+}$ (**10**) in PhCN containing excess TFA, thus giving the overall sequence of steps shown in Scheme 4.

Clear electrochemical evidence for the mechanism presented in Scheme 4 is given in Figure 7a for the fully protonated **10** whose reductions were investigated as a function of scan rate in a PhCN solution containing 250 equiv of TFA. The ratio of cathodic peak currents between the second and first reduction of **10** (i_{p2}/i_{p1}) approaches 1.0 at
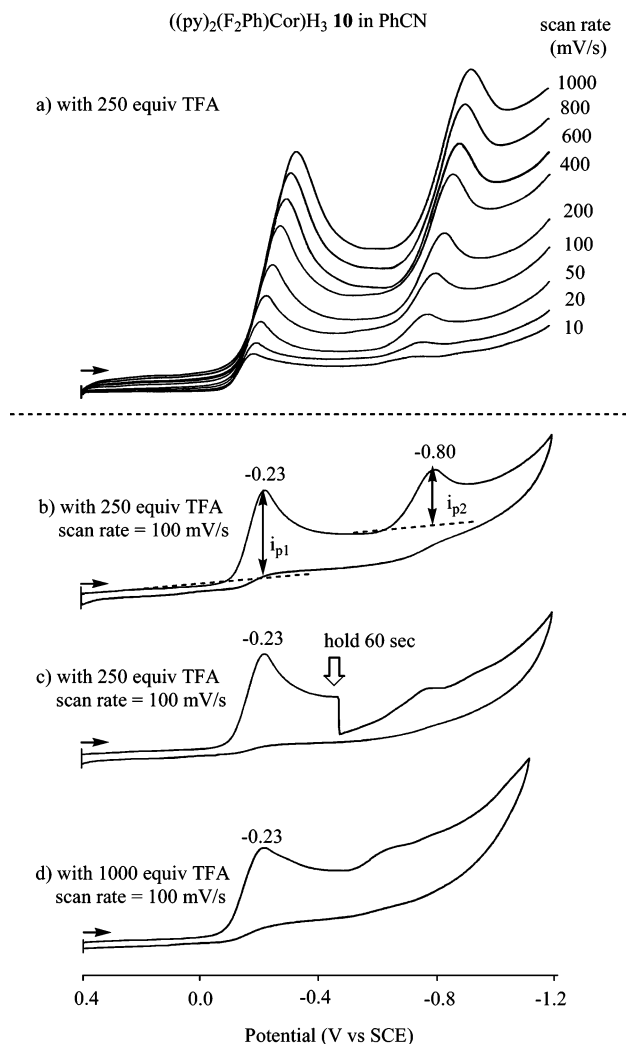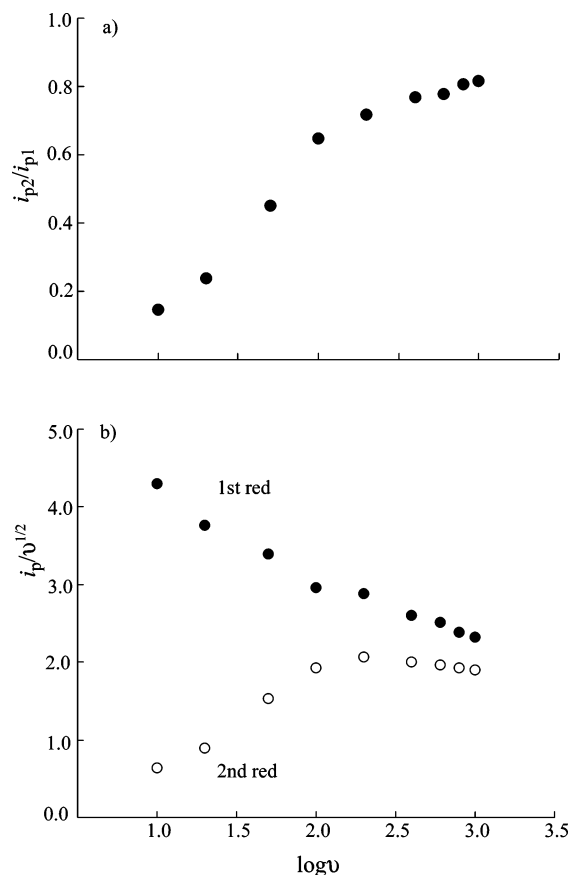
Figure 7. Cyclic voltammograms of protonated **10** in PhCN containing 0.1 M TBAP.
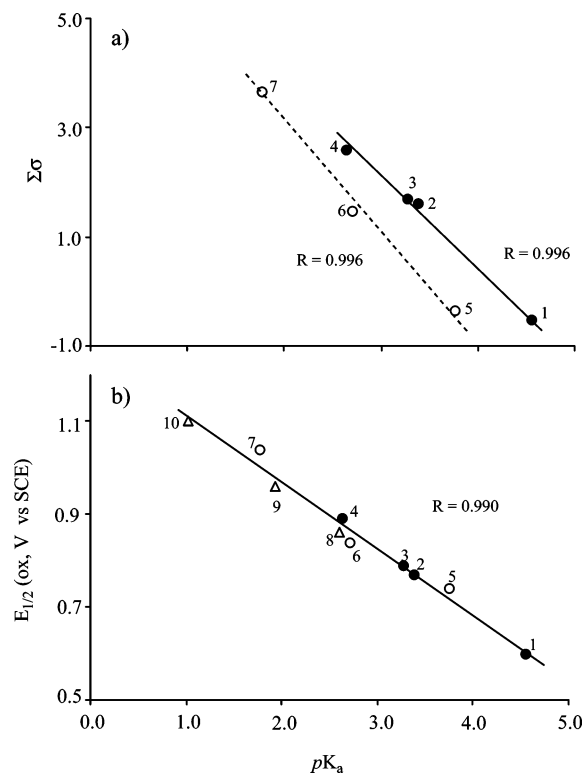

Figure 8. Scan rate dependence of (a) i_{p2}/i_{p1} and (b) $i_p/v^{1/2}$ for each reduction of protonated **10** in PhCN containing 0.1 M TBAP and 250 equiv of TFA. The value of v is given in mV/s.

the higher scan rates but is close to zero at low scan rates, as shown in Figures 7a and 8a.

At all scan rates, the initial electroreduction of **10** involves a one-electron conversion of $[(pyH^+)_2(Cor)H_4]^{3+}$ to $[(pyH^+)_2(Cor)H_4]^{2+}$ (the E step in Scheme 4) followed by a fast catalytic reduction of H^+ from the central nitrogens and formation of $[(pyH^+)_2(Cor)H_3]^{2+}$ at the electrode surface (the C step in Scheme 4). The product of the EC mechanism can then be re-protonated to give $[(pyH^+)_2(Cor)H_4]^{3+}$, as described in earlier sections of this manuscript, or it can be further reduced by a second electron at a more negative potential to give $[(pyH^+)_2(Cor)H_3]^+$ and then $[(pyH^+)_2(Cor)H_2]^+$ after a second chemical reaction, as shown in Scheme 4. The actual concentration of $[(pyH^+)_2(Cor)H_3]^{2+}$ at the electrode surface after the initial EC process will depend upon the potential scan rate, and this will be reflected by changes in the $i_p/v^{1/2}$ values for the two reductions, as shown in Figure 8b.

The peak currents for the second reduction of compound **10** will also depend upon the concentration of TFA added to solution. These currents are well-defined in PhCN containing 250 equiv of TFA for a scan rate of 100 mV/s (Figure 7b) but become negligible when the scan was held

for 60 s at potentials between the first and second reduction (Figure 7c) or when the TFA concentration was increased from 250 to 1000 equiv at a scan rate of 0.1 V/s (Figure 7d). The second reduction of protonated **10** is also barely seen at low potential scan rates of 10−20 mV/s (Figure 7a). Under these latter experimental conditions, the prevailing process then occurs as shown in the boxed portion of Scheme 4.

The mechanism shown in Scheme 4 applies to compounds **1**−**7**, which have no meso pyridyl substituents. It also applies to compounds **8** and **9**, which have one meso pyridyl substituent. The mono- and diprotonated corroles are all harder to reduce than the triprotonated **10**, and under these conditions, the second one-electron reduction is proposed to overlap in potential with the first process, leading to an apparent overall two-electron transfer.

Substituent Effect on pK_a Values. As indicated in the Experimental Section, the calculated pK_a values in Table 1 are only relative values because a definitive K_a for TFA is not available in PhCN, the only measurement being in H_2O.[20] The pK_a values of the 10 investigated corroles do, however, give an indication of how the acidity of each protonated corroles compare to each other. The calculated pK_a values range from 1.03 to 4.56 for deprotonation of the central nitrogens of compounds **1**−**10** (see p$K_{a(CN)}$ listed in Table 1).

It was anticipated that the measured pK_a values of compounds **1**−**10** could be related to other properties of the
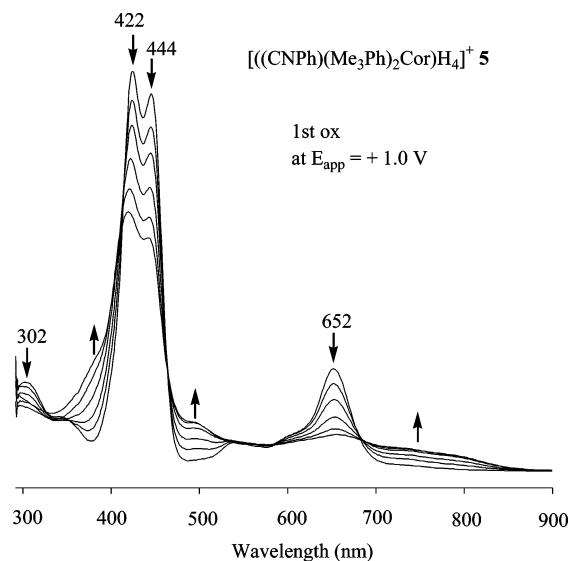
Figure 10. Thin-layer UV−visible spectral changes of [((CNPh)(Me₃-Ph)₂Cor)H₄]⁺ (**5**) during controlled potential oxidation at $E_{app} = +1.0$ V in PhCN containing 0.1 M TBAP.

Figure 9. Relationship between pK_a and (a) Σσ or (b) $E_{1/2}$ (ox) for fully protonated corroles, [(Cor)H₄]⁺ (**1−7**), [(Cor)H₅]²⁺ (**8** and **9**), and [(Cor)-H₆]³⁺ (**10**).

protonated corroles, the two most obvious of which are the reversible oxidation potentials and the Hammett constants on the meso substituents of the compounds, both of which reflect the electron density on the π-conjugated system and the four central nitrogens of the macrocycle. In our initial study of [(Cor)H₄]⁺, we showed that a single linear relationship was not observed between $E_{1/2}$ for oxidation of the protonated corroles and the sum of the substituent constants, Σσ, but rather two linear plots were observed.[2] One was for corroles with sterically hindered meso substituents and the other for corroles with nonsterically hindered meso substituents.[2] The same trend (two distinctly separate linear plots) is observed in the present study when correlating pK_a values and the Σσ of the substituents. One linear correlation is with **1−4** and the other with **5−7,** both of which have an $R = 0.996$. These plots are shown in Figure 9a and do not include compounds **8**, **9**, and **10** since a σ value is not available in the literature for the pyridyl substituents.

Surprisingly, a plot of $E_{1/2}$ for oxidation of the fully protonated corroles and the measured pK_a values shows only a single linear correlation with $R = 0.990$ for all 10 compounds. This plot is shown in Figure 9b and is especially interesting in that the correlation between $E_{1/2}$ and pK_a is independent of the structure of the compounds (hindered or nonhindered substituents), as well as independent of overall charge of the macrocycle which ranges from +1 in the case of **1−7** to +3 in the case of **10**.

Spectroelectrochemistry of Fully Protonated Corroles. The four fully protonated corroles **5**, **8**, **9**, and **10** were oxidized and reduced in a thin-layer cell in order to obtain the UV−visible spectra after controlled potential addition

or abstraction of electrons. Unfortunately, the spectral changes during controlled potential reduction could not be measured for the protonated **5**, **8**, and **9** derivatives due to the presence of large currents associated with the proposed catalytic reduction of protons in the thin-layer cell (see Scheme 4). Only the spectral changes of protonated **10** could be followed, and these spectral changes are shown in Figure S4.

In contrast to the reductions, well-defined spectral changes could be observed during controlled potential electrooxidation in the thin-layer cell, and examples of the obtained time-resolved spectra are shown in Figures 10−12 for protonated group A compound **5**, group B compound **8**, and group C compound **10**, respectively. The most straightforward spectral changes are seen during controlled potential oxidation of [((Me₃Ph)₂(CNPh)Cor)H₄]⁺ (**5**). Upon application of 1.0 V, the split Soret band at 422 and 444 nm and the visible band at 652 nm decrease in intensity and three new broad bands appear at ∼380, 490, and ∼750 nm. These changes are illustrated in Figure 10, and the final UV−visible spectrum at the completion of electrolysis is assigned as a π-cation radical of the protonated corrole. The same initial spectrum of [((Me₃Ph)₂(CNPh)Cor)H₄]⁺ (**5**) could be recovered when the controlled potential was set back to 0.0 V, thus indicating that the electron abstraction is reversible and that the product of the one-electron oxidation is stable on the thin-layer spectroelectrochemical time scale.

The spectral changes obtained during the first oxidation of fully protonated corroles **8−10** differ from that of **5** in that two well-defined sets of spectral transitions are seen as shown in Figure 11 for the group B compound **8** and Figure 12 for the group C compound **10**. The first set of spectral changes show isosbestic behavior from 0 to 192 s of electrolysis for compound **8** and from 0 to 126 s of electrolysis for **10**, both of which are reversible. The second set of spectral changes with isosbestic behavior occurs at longer electrolysis times of 192−622 s for **8** and 126−381 s for **10**, and here
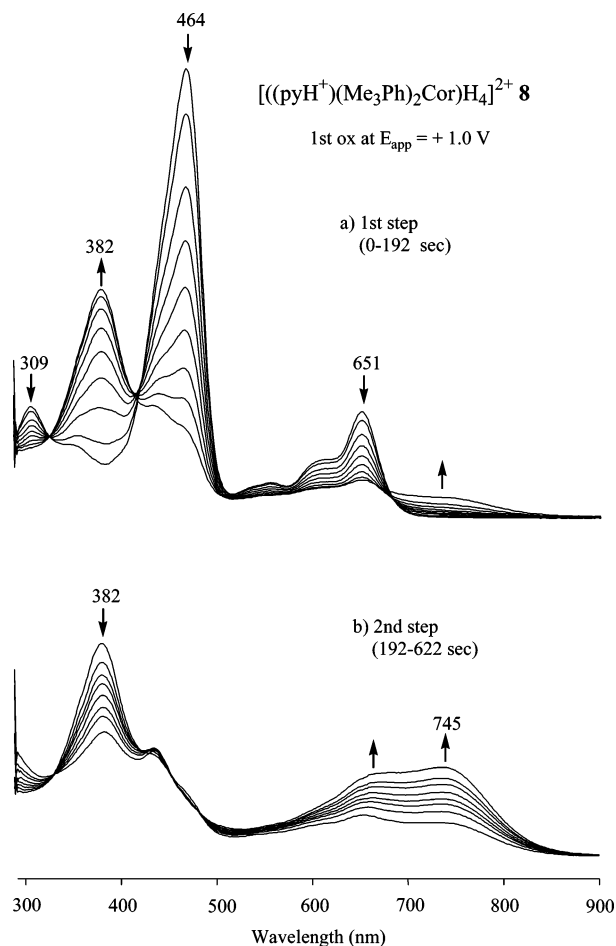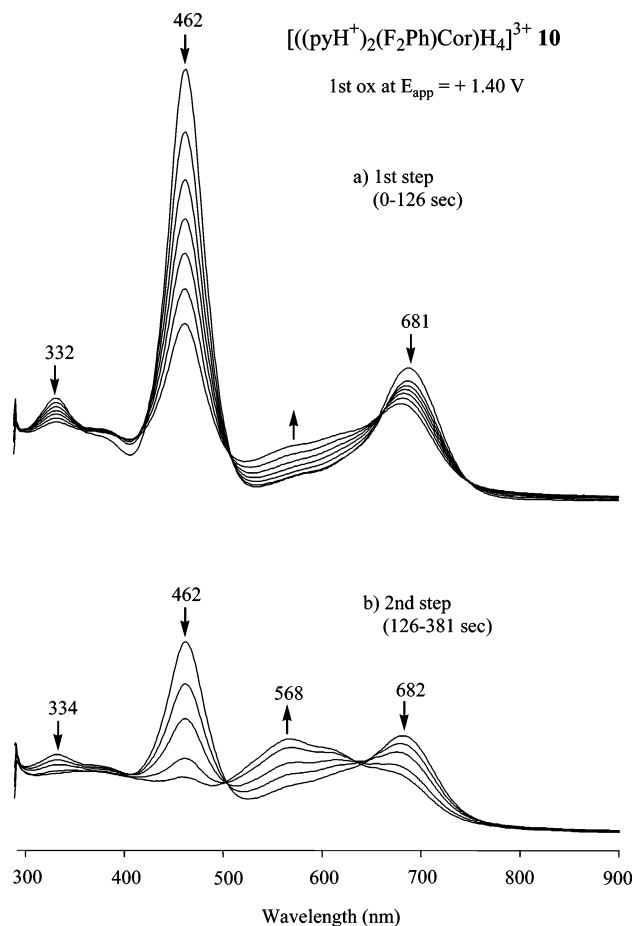
Figure 11. Thin-layer UV−visible spectral changes of $[((pyH^+)(Me_3Ph)_2Cor)H_4]^{2+}$ (**8**) during controlled potential oxidation at 1.0 V. The first step illustrated changes during the electron transfer, while the second show the changes during a followed coupled chemical reaction.

Figure 12. Thin-layer UV−visible spectral changes of $[((pyH^+)_2(F_2Ph)-Cor)H_4]^{3+}$ (**10**) during controlled potential oxidation at 1.40 V. The first step illustrated changes during the electron transfer, while the second show the changes during a followed coupled chemical reaction.

both processes are irreversible. These results are consistent with a slow chemical reaction following the initial electron abstraction from $[(Cor)H_5]^{2+}$. Compound **9** shows similar spectral changes as observed for **8**, and the relevant UV−vis spectra are illustrated in Figure S5.
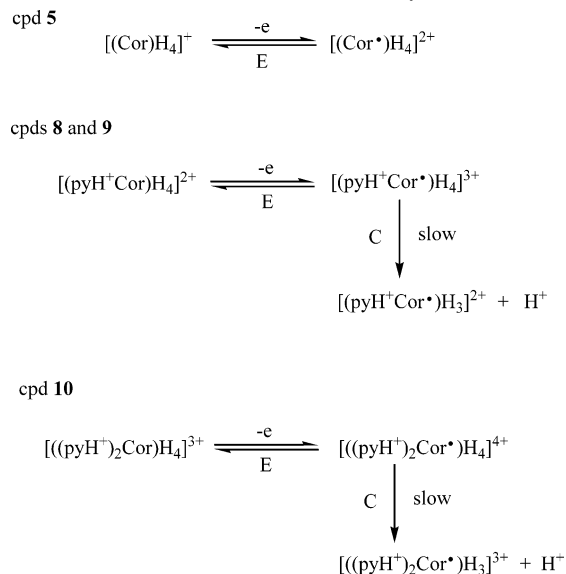
The chemical reaction following oxidation of the fully protonated compounds **8**, **9**, and **10** is proposed to involve a dissociation of one proton from the central nitrogens of the electrooxidized macrocycle, thus leading to the proposed mechanism shown in Scheme 5. The last proton added to the central nitrogens of the non-oxidized corroles **8**, **9**, and **10** (see Schemes 2 and 3) are only weakly bound, as indicated by the relatively small log *K* values of 2.38, 1.71, and 0.80 (Table 2). Protonation of the central nitrogens in these three compounds should then become even less favorable after formation of the cation radical, thus leading to the loss of a proton from the more highly charged complexes, $[((pyH^+)-Cor^\bullet)H_4]^{3+}$ (**8** and **9**) and $[((pyH^+)_2Cor^\bullet)H_4]^{4+}$ (**10**).

In summary, this paper presents the first spectroscopic data of electrooxidized free-base corroles in acidic nonaqueous media. Three types of protonated corroles were examined by thin-layer spectroelectrochemistry in PhCN/TFA mixtures, and these are represented as $[(Cor)H_4]^+$, $[(Cor)H_5]^{2+}$, and $[(Cor)H_6]^{3+}$. All of the compounds could be protonated on the central nitrogens of the macrocycle, but three corroles

Scheme 5. Electrooxidation Mechanism of Fully Protonated Corroles

cpd **5**

$$[(Cor)H_4]^+ \underset{E}{\overset{-e}{\rightleftharpoons}} [(Cor^\bullet)H_4]^{2+}$$

cpds **8** and **9**

$$[(pyH^+Cor)H_4]^{2+} \underset{E}{\overset{-e}{\rightleftharpoons}} [(pyH^+Cor^\bullet)H_4]^{3+}$$

$$C \bigg\downarrow \text{slow}$$

$$[(pyH^+Cor^\bullet)H_3]^{2+} + H^+$$

cpd **10**

$$[((pyH^+)_2Cor)H_4]^{3+} \underset{E}{\overset{-e}{\rightleftharpoons}} [((pyH^+)_2Cor^\bullet)H_4]^{4+}$$

$$C \bigg\downarrow \text{slow}$$

$$[((pyH^+)_2Cor^\bullet)H_3]^{3+} + H^+$$

with one or two meso pyridyl substituents underwent multiple protonation, both at the central nitrogens and at the nitrogens of the pyridyl substituents. The pK_a values for each protonated compound were measured and correlations examined between pK_a and the sum of the Hammett constants of the substituents on the meso positions of the corrole. A relation-

ship was also observed between the pK_a values and the oxidation potentials for the fully protonated corroles.

Supporting Information Available: UV−visible spectra of neutral and protonated corroles **1**−**10** in PhCN (Figure S1−S3), UV−visible spectral changes during the first reduction of fully protonated **10** (Figure S4) and during the first oxidation of fully protonated **9** (Figure S5). This material is available free of charge via the Internet at http://pubs.acs.org.

IC0617893